Published in final edited form as:
J Nucl Med. 2013 November ; 54(11): 1902–1908. doi:10.2967/jnumed.112.118125.

Evaluation of the Biodistribution of [^{11}C]Methionine in Children and Young Adults

Sebastian M. Harris[1,*], **James C. Davis**[1,**], **Scott E. Snyder**[1], **Elizabeth R. Butch**[1], **Amy L. Vāvere**[1], **Mehmet Kocak**[2,3], and **Barry L. Shulkin**[1]

[1]Department of Radiological Sciences, St. Jude Children's Research Hospital, Memphis, TN 38105

[2]Department of Biostatistics, St. Jude Children's Research Hospital, Memphis, TN 38105

[3]Department of Preventive Medicine, University of Tennessee Health Science Center, Memphis, TN, 38105

Abstract

The purpose of this study was to evaluate the biodistribution of carbon-11–labeled methionine in non–tumor-involved organs in pediatric patients studied for malignant diseases.

Methods—Ninety-three children and young adults with known or suspected malignancies underwent [^{11}C]methionine positron emission tomography (PET) and computed tomography (CT) scans. Imaging began 5–15 min after injection of 740 MBq (20 mCi) per 1.7 m^2 of body surface area. Images were acquired from the top of the head through the mid-thighs. Standardized uptake values were determined using regions of interest drawn on the CT and transferred to the corresponding transverse PET slice.

Results—The highest concentrations of [^{11}C]methionine were found in the pancreas and liver. Less intense uptake was seen in other regions, such as salivary glands, tonsils, and bone marrow. There was very little uptake in lungs, fat (including brown adipose tissue), and muscle. Uptake in bone marrow, parotid glands, and tonsils was slightly but statistically significantly higher in males than females. Testicular, bone marrow, and left ventricular uptake increased with age. There was little variability statistically between comparisons of uptake change and groupings of age, race, sex, and patients studied at the time of diagnosis versus previously treated patients.

Conclusion—High uptake of [^{11}C]methionine is reliably found in the pancreas and liver, consistent with the anabolic functions of these organs. Low uptake in the brain, neck, chest, pelvis, and extremities will facilitate tumor localization in those areas. However, intense uptake in the upper abdomen may limit the diagnostic utility of [^{11}C]methionine in that area.

Keywords

PET/CT; carbon-11; methionine; pediatric; tumor

INTRODUCTION

The most commonly used radiotracer for the staging and monitoring of neoplastic disease is [^{18}F]fluorodeoxyglucose (FDG) (1). Elevated FDG uptake is common in many tumors, and

Corresponding author: Barry L. Shulkin, MD, St. Jude Children's Research Hospital, Department of Radiological Sciences, 262 Danny Thomas Place, MS 220, Memphis, TN 38105-3678, Phone: 901-595-3347, Fax: 901-595-3981.
*College of Medicine, University of Oklahoma Health Science Center, Oklahoma City, OK 73117
**School of Medicine, University of Tennessee Health Science Center, Memphis, TN 38163

FDG positron emission tomography (PET) with computed tomography (CT) is frequently used in the management of patients with lung tumors, lymphomas, melanomas, and others (2–4). However, there are limitations to its use. FDG uptake in brain tumors is complicated by intense background activity in the cerebral cortex, thus limiting its use in monitoring low-grade gliomas (5). In addition to central nervous system (CNS) tumors, FDG has limited utility for the study of bronchioloalveolar carcinomas, renal cell carcinomas, bladder tumors, prostate cancer, and others (6–8). FDG uptake is also a feature of some non-neoplastic conditions, such as inflammation and infection (9). Thus, new radiotracers are being developed to overcome the limitations and drawbacks of FDG in certain clinical conditions.

Methionine, a naturally occurring essential amino acid, can be labeled with the positron-emitting isotope carbon-11 and studied using PET scanning. Methionine, which is transported into cells via the L-type amino acid transporter 1 (LAT1) is crucial for the formation of proteins and is involved in the synthesis of phospholipids. The formation of proteins is an integral part of cellular growth and replication. As cells replicate, the demand for protein and phospholipid synthesis increases, rendering transport and reclamation of essential amino acids crucial for tumor growth. Methionine has been found to accumulate in a variety of tumors (10–12). In particular, for non-small cell lung carcinomas, the uptake of methionine closely correlates with cellular replication (11). In gliomas, uptake of methionine correlates with both cellular proliferation and microvessel density (12).

The pharmacokinetics and dosimetry for [^{11}C]methionine in adult humans have been reported by Deloar et al. (13) based on whole-body PET data. The pancreas, liver, bladder, and kidney showed the greatest initial uptake of [^{11}C]methionine. The subjects in that study underwent scanning at multiple time points for calculation of dosimetry. The pancreas and liver had the highest retention of activity among the organs studied.

In this study, we examined the biodistribution of [^{11}C]methionine in non–tumor-involved organs of young patients with newly diagnosed neoplasms and patients with secondary or recurrent neoplasms of childhood. Specifically, we examined methionine uptake variability across age, sex, and race. Uptake in organs not containing tumors was assessed and semiquantitatively evaluated to document the normal biodistribution of the tracer in children and young adults. We also compared uptake between patients with newly diagnosed malignancies who had not begun treatment and those who had recurrent tumors and were candidates for further antineoplastic therapy (radiation, chemotherapy, or both) for their primary malignant neoplasm. Patients with recurrent disease had not received therapy for at least 90 days,

MATERIALS AND METHODS

Patients

Patients (n=93) with known or subsequently proven neoplastic disease were studied from July 2009 to July 2011. Demographic data are summarized in Table 1. Of 93 patients, there were 55 males (60%) and 38 females (40%). Ages ranged from 2 to 29 years (median 12). Inclusion criteria for patient enrollment had no limits on age, sex, race, or type of diagnosis. Patients with newly diagnosed disease who had not yet undergone therapy (n = 62) and those with recurrent disease who had not received treatment in 3 or more months (n = 31) were included. Major diagnoses were CNS tumors (n=43), sarcomas (n=19), lymphomas (n=8), carcinomas (n=8), and others (n=15, including Wilms tumors and neuroblastoma). Although many patients subsequently underwent multiple scans, only data from the baseline study were included. The St. Jude Children’s Research Hospital institutional review board approved this study and all subjects and/or one or both of their parents signed a written informed consent document.

Radiochemistry

For this study, [^{11}C]methionine was produced by the method of Ishiwata et al. (14), starting from [^{11}C]methyl iodide and *L*-homocysteine thiolactone, and adapted for preparation on a PETChem Solutions (East Lansing, MI) automated synthesis module. This method has been shown to produce <3% *D*-[^{11}C]methionine. For a detailed description of the radiochemistry, see Vavere and Snyder (15).

PET/CT Technique

Before imaging, participants fasted for at least 4 h. Patients were then given intravenous injections of 740 MBq (20 mCi) of [^{11}C]methionine per 1.7 m^2 of body surface area (maximum prescribed dose, 740 MBq). Transmission CT images, for attenuation correction and lesion localization, and PET images were acquired approximately 5–15 min later using a GE Discovery LS PET/CT system (GE Medical Systems, Waukesha, WI). CT acquisition parameters were slice thickness of 0.5 cm, 0.8 s tube rotation, table speed 1.5 cm/rotation, pitch 1.5:1, 120 kV, 90 mA, with dose modulation. PET images were obtained from the top of the skull through the mid-thighs for 3 min per bed position in 2D mode. Data were reconstructed into multiplanar cross-sectional images using standard vendor-supplied software and displayed on a nuclear medicine workstation (HERMES Medical Solutions, Chicago, IL) for analysis.

Image and Data Analysis—Standardized uptake values for the structures listed in Table 2 were determined using regions of interest drawn on selected CT images, and then transferred to the corresponding PET image in the transverse plane.

The number of selected ROIs per patient varied slightly due in some cases to complete resection of a specific tissue or organ or due to organ involvement by diseased tissue. Table 2 accounts for this discrepancy and reports the actual number of data points used per selected tissue or organ and statistical analysis including minimum, first quartile, median, third quartile, and maximum SUV.

Graphical and descriptive statistics were used to display and compare methionine SUVmax data. The median SUV for a given ROI was used for statistical analysis because this measurement is least affected by outliers. SUV distribution was statistically compared among subgroups of patients using the Wilcoxon-Mann-Whitney test, a non-parametric counterpart of the two-sample *t*-test. Comparisons of SUV by location, between right and left for paired organs, within sites for the lungs and vertebral bodies, between newly diagnosed patients and those with recurrent disease, and by age were performed. Association of age at scan time and SUV was investigated using Spearman's rank correlation. Results were considered significant at a *P*-value limit of 0.05 or less in a hypothesis generating context, and the *P*-values reported were not adjusted for multiplicity.

RESULTS

The highest accumulation of [^{11}C]methionine was found in the pancreas and liver, both of which were readily recognizable as areas of prominent activity on emission images (Fig. 1; Table 2). The median SUVmax was 12.4 in the pancreas and 8.5 in the liver. There were no statistical differences between lobes of the liver or between pairs of other organs examined, including the tonsils, salivary glands, kidneys, and lungs (Figs. 1 – 6). Activity was evident in Waldeyer's ring lymphoid tissue, submandibular glands, bone marrow, and kidneys. Activity was visually homogenous in most organs. Intestinal uptake was quite variable in intensity, extent, and location and could not be quantified further due to the imprecision of localization on non-contrast, low-resolution CT scans.

Newly Diagnosed Versus Not Newly Diagnosed

There were very few and minor differences in biodistribution between patients with newly diagnosed disease and patients with previously treated disease. Uptake in T4 and T5 vertebral bodies in previously treated patients was slightly less (T4, median, 1.93. vs. 2.48, $P = 0.0034$; T5, median, 2.03 vs. 2.38, $P = 0.0077$) (Fig. 7) than in untreated patients. None of the differences in other regions reached a P value of 0.01, although the pattern for T6, $P = 0.06$, was similar to that seen in T4 and T5.

Sex Comparisons

Male and female patients compared by median SUV showed a modest number of statistically variant tissues and organs. In the tonsillar tissues of Waldeyer's ring and in the salivary glands (parotid and submandibular), uptake was greater in males than females (P values ranged from 0.0009 to 0.026). The vertebral bodies showed greater uptake in males than females, although only T10 and T5 were statistically significant ($P = 0.0075$ and 0.0079, respectively) (Fig. 8).

Dosimetry

Dosimetry was calculated for age groups using data provided in reference (16) (Table 3).

Age Comparisons

The uptake in many regions increased slightly with age. These areas included the testicles ($P < 0.0001$) (Figure 9), the liver ($P < 0.0001$), left ventricular myocardium ($P = 0.0002$), and multiple vertebral bodies.

DISCUSSION

In our study of pediatric patients undergoing [^{11}C]methionine studies for malignancies, the pancreas and liver consistently showed the greatest uptake of [^{11}C]methionine. This is similar to the findings of Deloar et al. (13), who described high uptake and retention of [^{11}C]methionine in the pancreas and liver of 5 adult healthy volunteers. The exocrine pancreas produces enzymes, such as trypsin and chymotrypsin, for the breakdown of ingested proteins, fats, and carbohydrates. Similarly, the liver requires amino acids for the synthesis of plasma proteins, such as albumin, fibrinogen, and transferrin. Thus, the high uptake in both these organs may reflect the need for methionine and other large neutral amino acids for protein synthesis.

Among the tissues and organs analyzed for [^{11}C]methionine uptake, bone marrow in the axial skeleton was consistently prominent. This is likely due to the demand for protein synthesis in the replicating cells in the bone marrow. The vertebral bodies analyzed showed small but statistically significant differences based on age, sex, and newly diagnosed versus not newly diagnosed disease. This suggests that axial bone marrow uptake increases slightly with age and is slightly greater in males than females. The small differences between patients who had been treated and not treated may reflect a slight decline in bone marrow reserve in patients who have been previously exposed to a variety of antineoplastic agents.

The left ventricle had greater uptake in males than in females. In addition, uptake in the left ventricle increased over time. This could be due to a greater average body mass in males than in females and an increase in body mass over time. Methionine increases contractility of the heart by N-methlylation of membrane phospholipids of the sarcoplasmic reticulum and sarcollema (17). The parotid glands showed a pattern of uptake similar to that in the left ventricle for sex and age, although the changes were quite small.

The data on biodistribution of [^{11}C]methionine in adult patients are limited principally to analysis of tumor uptake. Nonetheless some non tumor organ uptake has been described. The median SUVmax in T11 of our patients, 2.0, was similar to the mean SUVmax of T11 in 10 adult control patients with hyperparathyroidism, 1.8 ± 0.3 (18). These values are lower than the vertebral body uptake described by Netterbladt (19). In that study, vertebral body uptake was 4.2 ± 1.3 in 17 patients with lung and mediastinal tumors. Liver uptake in our study, SUVmax ~8.5 averaging both lobes, was lower than that in the study of Netterbladt, SUVmax 11.2 ± 2.2, and lower than that found in a study of 10 patients with malignant melanoma, 12.6 ± 3.6 (4 patients had only liver measurements) (20). In the latter study, salivary gland uptake was 5.9 ± 1.3 (3 patients), compared with our findings of ~3.0 for submandibular glands and 2.5 for parotid glands. Lung uptake in the study of Netterbladt (19), 0.6 ± 0.1, was quite close to the 0.6–0.7 found in our study.

There were limitations to our study. For practical reasons, scanning was performed at only a single time point after injection; thus, dynamic organ uptake and retention could not be assessed. The time to the start of body imaging of patients also studied for CNS disease was longer than those studied for extracranial involvement because the body imaging occurred after a dedicated brain study. However, Deloar et al. (13) showed that the uptake of methionine occurs quite quickly and that the decline in activity over time was due to physical decay. Thus, the retention of tracer was quite high with very little efflux during the time of imaging. This indicates that the small differences in the time intervals from injection to imaging should not affect our results. Intra-subject reproducibility could not be assessed for practical and ethical concerns of scheduling and performing repeat scans before initiation of further treatment.

The calculated dosimetry (Table 3) shows that the EDE (effective dose equivalent) ranged from 5.8 to 6.9 mSv. The target organ is the bladder wall, followed by the kidneys, pancreas, and liver. The bladder contributes 65% of EDE (16). The calculated value for the bladder wall, 81mSv for an adult, may represent a considerable overestimation of absorbed dose, as the data of Deloar indicate a value of 20 mSv. Newer scanners with 3D acquisition and other features of modern PET/CT cameras may allow dose reduction yet preserve or enhance image quality. Fluid administration to promote diuresis, early voiding and/or bladder catheterization may also reduce bladder and thereby patient exposure.

The principal tumors studied with [^{11}C]methionine have been CNS neoplasms, which have been studied for more than 20 years. Unlike with FDG, which is normally concentrated within the brain, particularly cerebral gray matter, the brain shows very little uptake of [^{11}C]methionine under normal circumstances (21). O'Tuama et al. (22) examined 13 children, ages 1.8–15.8 years, with brain tumors using [^{11}C]methionine. This was the first documented report of [^{11}C]methionine in childhood brain tumors. Increased [^{11}C]methionine was found in the tumors of 11 of the 13 patients. Other studies have also shown utility for [^{11}C]methionine for the study of childhood and adult brain tumors (23–25). The regional uptake of [^{11}C]methionine in normal brain tissue has been described by Coope et al. (26). The highest uptake was found in the cerebellum and occipital cortex, with less in white matter. The study of Nagata also showed high uptake in the cerebellum of normal children and increasing SUV in the frontal lobes and cerebellum with age (27).

Non-CNS tumors have been studied less extensively. These include bronchogenic carcinomas, melanomas, multiple myeloma, colorectal carcinomas, hepatomas, ovarian and uterine tumors, and bladder and prostate carcinomas (18–20,28–30). Parathyroid adenomas have been successfully localized using [^{11}C]methionine (31).

Methionine, along with other neutral amino acids that have large, branched or aromatic side chains, such as leucine, isoleucine, phenylalanine, tyrosine, histidine, tryptophan, and valine, are transported into cells by LAT1 (32). LAT1 is Na^+-independent and functions as an amino acid exchanger (33). It consists of 507 amino acids with a molecular weight of ~55 kDa and 12 transmembrane-spanning non-glycoproteins (34,35). LAT1 is also the transporter for amino acid–related molecules such as L-dopa, thyroxine, and tri-iodothyronine, as well as the chemotherapeutic agent melphalan (L-phenylalanine mustard) (36). LAT1 is found in brain, placenta, and liver, and it is overexpressed in many types of tumors (33,37–40), including gliomas, gastric carcinomas, non-small cell carcinomas of the lungs, and esophageal carcinoma. Inhibition of LAT1 has been reported to have antitumor activity in vitro and in vivo (35). If effective therapies using LAT1 inhibitors are developed, it is possible that [^{11}C]methionine could serve as a method to assess antitumor efficacy.

CONCLUSION

We have explored the biodistribution of [^{11}C]methionine in non–tumor-involved organs in children and young adults with known or suspected malignancies. The high uptake within the pancreas and liver suggests that their background activity may impair the search for neoplasms in the abdomen. Relatively low uptake of this agent in brain tissue facilitates tumor localization in the brain. Low background in the neck, chest, and extremities will likely facilitate tumor localization in those regions.

Acknowledgments

The authors thank Sandra Gaither for secretarial expertise and David Galloway of Scientific Editing for editorial support. The authors are grateful to the Molecular Imaging Research laboratory staff for production of [^{11}C]methionine. Funded in part by Award Number 5R25CA023944 from the National Cancer Institute (NCI) (authors SMH, JCD) and by generous support from the American Lebanese Syrian Associated Charities (ALSAC).

Reference List

1. Wahl, RL. Principles of cancer imaging with 18-F fluorodeoxyglucose (FDG). In: Wahl, RL., editor. Principles and Practice of PET and PET/CT. Philadelphia: Lippincott Williams and Williams; 2008. p. 117-130.
2. Weber WA, Petersen V, Schmidt B, et al. Positron emission tomography in non-small-cell lung cancer: prediction of response to chemotherapy by quantitative assessment of glucose use. J Clin Oncol. 2003; 21:2651–2657. [PubMed: 12860940]
3. Juweid ME, Cheson BD. Role of positron emission tomography in lymphoma. J Clin Oncol. 2005; 23:4577–4580. [PubMed: 15837974]
4. Reinhardt MJ, Joe AY, Jaeger U, et al. Diagnostic performance of whole body dual modality 18F-FDG PET/CT imaging for N- and M-staging of malignant melanoma: experience with 250 consecutive patients. J Clin Oncol. 2006; 24:1178–1187. [PubMed: 16505438]
5. Chung JK, Kim YK, Kim SK, et al. Usefulness of 11C-methionine PET in the evaluation of brain lesions that are hypo- or isometabolic on 18F-FDG PET. Eur J Nucl Med Mol Imaging. 2002; 29:176–182. [PubMed: 11926379]
6. Higashi K, Ueda Y, Seki H, et al. Fluorine-18-FDG PET imaging is negative in bronchioloalveolar lung carcinoma. J Nucl Med. 1998; 39:1016–1020. [PubMed: 9627336]
7. Kang DE, White RL Jr, Zuger JH, Sasser HC, Teigland CM. Clinical use of fluorodeoxyglucose F 18 positron emission tomography for detection of renal cell carcinoma. J Urol. 2004; 171:1806–1809. [PubMed: 15076281]
8. Schoder, H. Genitourinary malignancies. In: Wahl, RL., editor. Principles and practice of PET and PET/CT. Philadelphia: Lippincott Williams & Wilkins; 2008. p. 366-391.

9. Basu S, Zhuang H, Torigian DA, Rosenbaum J, Chen W, Alavi A. Functional imaging of inflammatory diseases using nuclear medicine techniques. Semin Nucl Med. 2009; 39:124–145. [PubMed: 19187805]
10. Zhang H, Yoshikawa K, Tamura K, et al. [(11)C]methionine positron emission tomography and survival in patients with bone and soft tissue sarcomas treated by carbon ion radiotherapy. Clin Cancer Res. 2004; 10:1764–1772. [PubMed: 15014030]
11. Miyazawa H, Arai T, Iio M, Hara T. PET imaging of non-small-cell lung carcinoma with carbon-11-methionine: relationship between radioactivity uptake and flow-cytometric parameters. J Nucl Med. 1993; 34:1886–1891. [PubMed: 8229229]
12. Kracht LW, Friese M, Herholz K, et al. Methyl-[11C]- l-methionine uptake as measured by positron emission tomography correlates to microvessel density in patients with glioma. Eur J Nucl Med Mol Imaging. 2003; 30:868–873. [PubMed: 12692687]
13. Deloar HM, Fujiwara T, Nakamura T, et al. Estimation of internal absorbed dose of L-[methyl-11C]methionine using whole-body positron emission tomography. Eur J Nucl Med. 1998; 25:629–633. [PubMed: 9618578]
14. Ishiwata K, Ido T, Abe Y, Matsuzawa T, Iwata R. Tumor uptake studies of S-adenosyl-L-[methyl-11C]methionine and L-[methyl-11C]methionine. Int J Rad Appl Instrum A. 1988; 39:311–314. [PubMed: 2838437]
15. Vavere, AL.; Snyder, SE. Synthesis of L-[methyl-11C]methionine ([11C]MET). In: Scott, PJ.; Hockley, B., editors. Radiochemical Syntheses. New York: John Wiley & Sons; 2012. p. 199-212.
16. ICRP. Radiation dose to patients from radiopharmaceuticals - addendum 3 to ICRP publication 53. ICRP publication 106. Ann ICRP. 2008; 38(1–2)
17. Pisarenko OI. Mechanisms of myocardial protection by amino acids: facts and hypotheses. Clin Exp Pharmacol Physiol. 1996; 23:627–633. [PubMed: 8886480]
18. Dankerl A, Liebisch P, Glatting G, et al. Multiple myeloma: molecular imaging with 11C-methionine PET/CT--initial experience. Radiology. 2007; 242:498–508. [PubMed: 17179397]
19. Nettelbladt OS, Sundin AE, Valind SO, et al. Combined fluorine-18-FDG and carbon-11-methionine PET for diagnosis of tumors in lung and mediastinum. J Nucl Med. 1998; 39:640–647. [PubMed: 9544671]
20. Lindholm P, Leskinen S, Nagren K, et al. Carbon-11-methionine PET imaging of malignant melanoma. J Nucl Med. 1995; 36:1806–1810. [PubMed: 7562047]
21. O'Tuama LA, Phillips PC, Smith QR, et al. L-methionine uptake by human cerebral cortex: maturation from infancy to old age. J Nucl Med. 1991; 32:16–22. [PubMed: 1988624]
22. O'Tuama LA, Phillips PC, Strauss LC, et al. Two-phase [11C]L-methionine PET in childhood brain tumors. Pediatr Neurol. 1990; 6:163–170. [PubMed: 2193641]
23. Ceyssens S, Van Laere K, de Groot T, Goffin J, Bormans G, Mortelmans L. [11C]methionine PET, histopathology, and survival in primary brain tumors and recurrence. AJNR Am J Neuroradiol. 2006; 27:1432–1437. [PubMed: 16908552]
24. Kaschten B, Stevenaert A, Sadzot B, et al. Preoperative evaluation of 54 gliomas by PET with fluorine-18-fluorodeoxyglucose and/or carbon-11-methionine. J Nucl Med. 1998; 39:778–785. [PubMed: 9591574]
25. Kim S, Chung JK, Im SH, et al. 11C-methionine PET as a prognostic marker in patients with glioma: comparison with 18F-FDG PET. Eur J Nucl Med Mol Imaging. 2005; 32:52–59. [PubMed: 15309332]
26. Coope DJ, Cizek J, Eggers C, Vollmar S, Heiss WD, Herholz K. Evaluation of primary brain tumors using 11C-methionine PET with reference to a normal methionine uptake map. J Nucl Med. 2007; 48:1971–1980. [PubMed: 18006617]
27. Nagata T, Tsuyuguchi N, Uda T, Terakawa Y, Takami T, Ohata K. Examination of 11C-methionine metabolism by the standardized uptake value in the normal brain of children. J Nucl Med. 2011; 52:201–205. [PubMed: 21270456]
28. Inoue T, Kim EE, Wong FC, et al. Comparison of fluorine-18-fluorodeoxyglucose and carbon-11-methionine PET in detection of malignant tumors. J Nucl Med. 1996; 37:1472–1476. [PubMed: 8790196]

29. Yasukawa T, Yoshikawa K, Aoyagi H, et al. Usefulness of PET with 11C-methionine for the detection of hilar and mediastinal lymph node metastasis in lung cancer. J Nucl Med. 2000; 41:283–290. [PubMed: 10688112]
30. Wieder H, Ott K, Zimmermann F, et al. PET imaging with [11C]methyl- L-methionine for therapy monitoring in patients with rectal cancer. Eur J Nucl Med Mol Imaging. 2002; 29:789–796. [PubMed: 12029553]
31. Sundin A, Johansson C, Hellman P, et al. PET and parathyroid L-[carbon-11]methionine accumulation in hyperparathyroidism. J Nucl Med. 1996; 37:1766–1770. [PubMed: 8917171]
32. Fuchs BC, Bode BP. Amino acid transporters ASCT2 and LAT1 in cancer: partners in crime? Semin Cancer Biol. 2005; 15:254–266. [PubMed: 15916903]
33. del Amo EM, Urtti A, Yliperttula M. Pharmacokinetic role of L-type amino acid transporters LAT1 and LAT2. Eur J Pharm Sci. 2008; 35:161–174. [PubMed: 18656534]
34. Mastroberardino L, Spindler B, Pfeiffer R, et al. Amino-acid transport by heterodimers of 4F2hc/CD98 and members of a permease family. Nature. 1998; 395:288–291. [PubMed: 9751058]
35. Oda K, Hosoda N, Endo H, et al. L-type amino acid transporter 1 inhibitors inhibit tumor cell growth. Cancer Sci. 2010; 101:173–179. [PubMed: 19900191]
36. Uchino H, Kanai Y, Kim DK, et al. Transport of amino acid-related compounds mediated by L-type amino acid transporter 1 (LAT1): insights into the mechanisms of substrate recognition. Mol Pharmacol. 2002; 61:729–737. [PubMed: 11901210]
37. Okubo S, Zhen HN, Kawai N, Nishiyama Y, Haba R, Tamiya T. Correlation of L-methyl-11C-methionine (MET) uptake with L-type amino acid transporter 1 in human gliomas. J Neurooncol. 2010; 99:217–225. [PubMed: 20091333]
38. Ichinoe M, Mikami T, Yoshida T, et al. High expression of L-type amino-acid transporter 1 (LAT1) in gastric carcinomas: comparison with non-cancerous lesions. Pathol Int. 2011; 61:281–289. [PubMed: 21501294]
39. Kaira K, Oriuchi N, Otani Y, et al. Fluorine-18-alpha-methyltyrosine positron emission tomography for diagnosis and staging of lung cancer: a clinicopathologic study. Clin Cancer Res. 2007; 13:6369–6378. [PubMed: 17975149]
40. Kobayashi H, Ishii Y, Takayama T. Expression of L-type amino acid transporter 1 (LAT1) in esophageal carcinoma. J Surg Oncol. 2005; 90:233–238. [PubMed: 15906366]

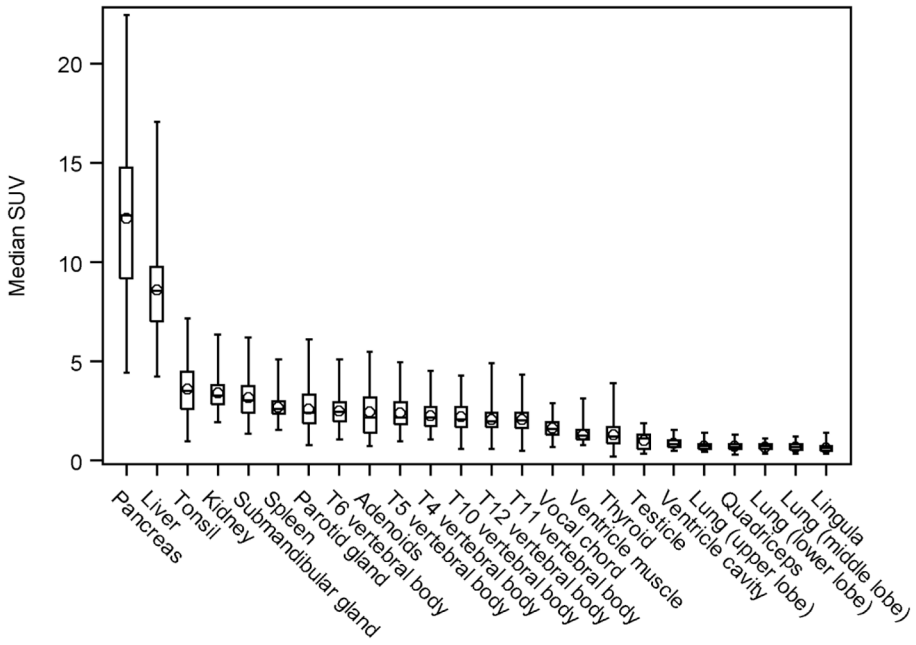

FIGURE 1.

The SUVs for the tissues examined. Individual data points are depicted, along with the group median (solid horizontal line in the rectangular box), the group mean (◇ symbol), the first and third quartiles above and below the group median (rectangular box), and the minimum and maximum SUV values (top and bottom horizontal lines.

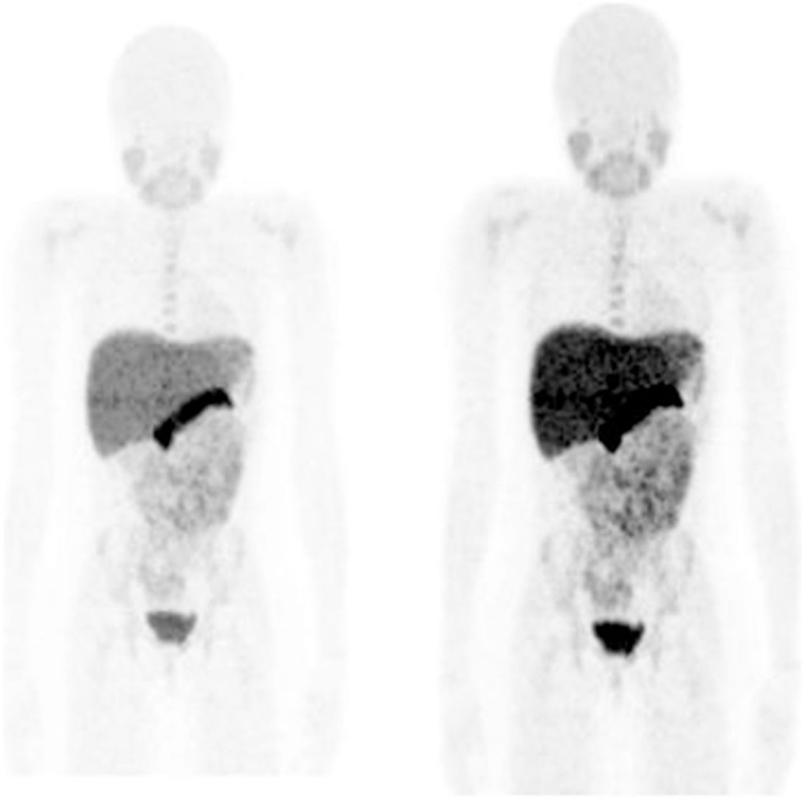

FIGURE 2.
Whole body anterior maximal intensity projection image of a 7-year-old girl studied for a cerebral neoplasm. Images are displayed at two different intensities to show relative distribution of the tracer. The pancreas and liver contain the highest concentrations.

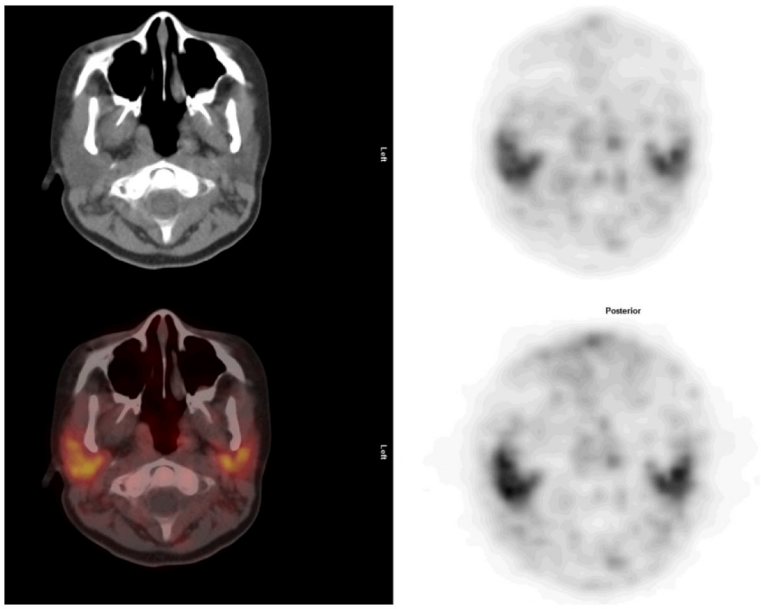

FIGURE 3.

Neck: Cross sectional representations of activity seen at various levels of the body. Upper row left column attenuation correction CT scan, upper row right column attenuation corrected PET image, lower row left column fusion image of CT and attenuation corrected PET image, and bottom right, non attenuation corrected PET image. The attenuation corrected PET image is scaled to a maximum SUV of 5.0.

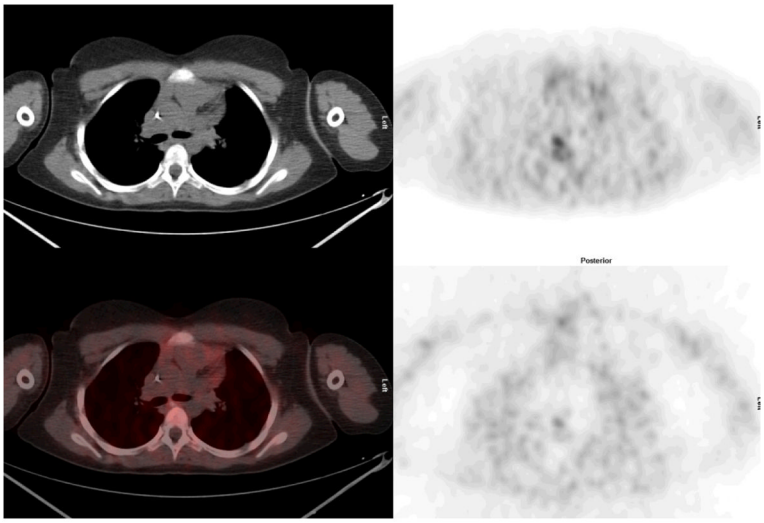

FIGURE 4.

Mid chest: Cross sectional representations of activity seen at various levels of the body. Upper row left column attenuation correction CT scan, upper row right column attenuation corrected PET image, lower row left column fusion image of CT and attenuation corrected PET image, and bottom right, non attenuation corrected PET image. The attenuation corrected PET image is scaled to a maximum SUV of 5.0.

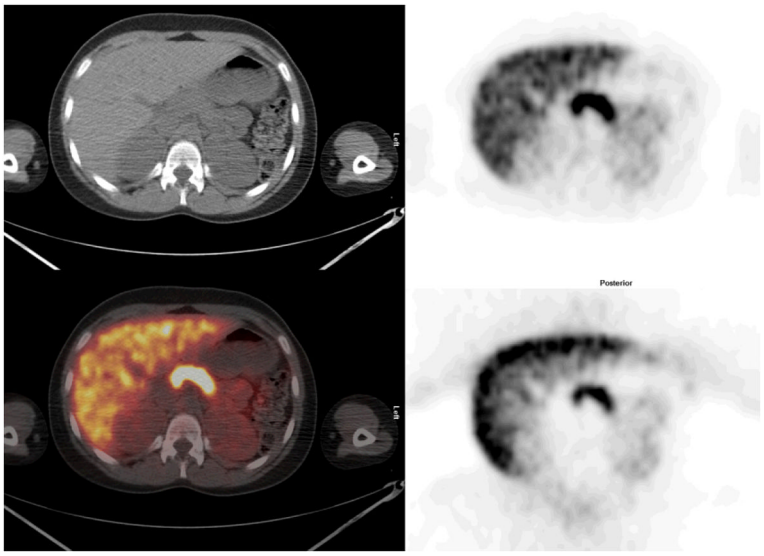

FIGURE 5.

Mid abdomen: Cross sectional representations of activity seen at various levels of the body. Upper row left column attenuation correction CT scan, upper row right column attenuation corrected PET image, lower row left column fusion image of CT and attenuation corrected PET image, and bottom right, non attenuation corrected PET image. The attenuation corrected PET image is scaled to a maximum SUV of 12.

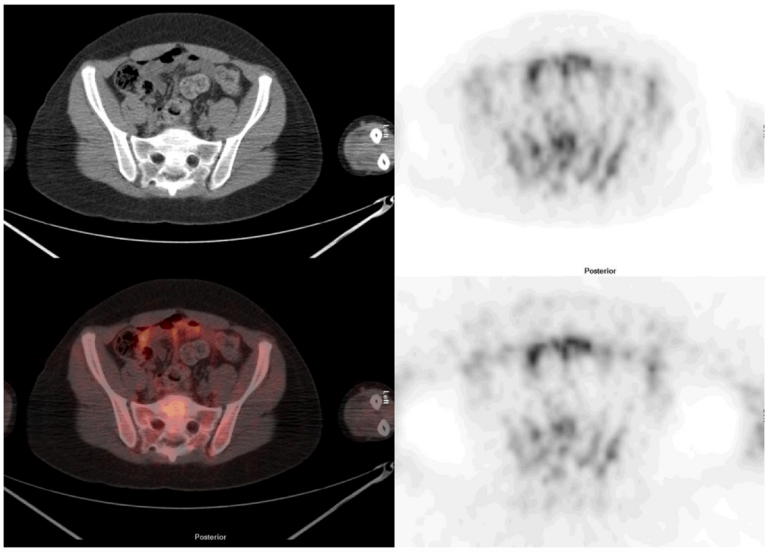

FIGURE 6.

Pelvis: Cross sectional representations of activity seen at various levels of the body. Upper row left column attenuation correction CT scan, upper row right column attenuation corrected PET image, lower row left column fusion image of CT and attenuation corrected PET image, and bottom right, non attenuation corrected PET image. The attenuation corrected PET image is scaled to a maximum SUV of 5.0.

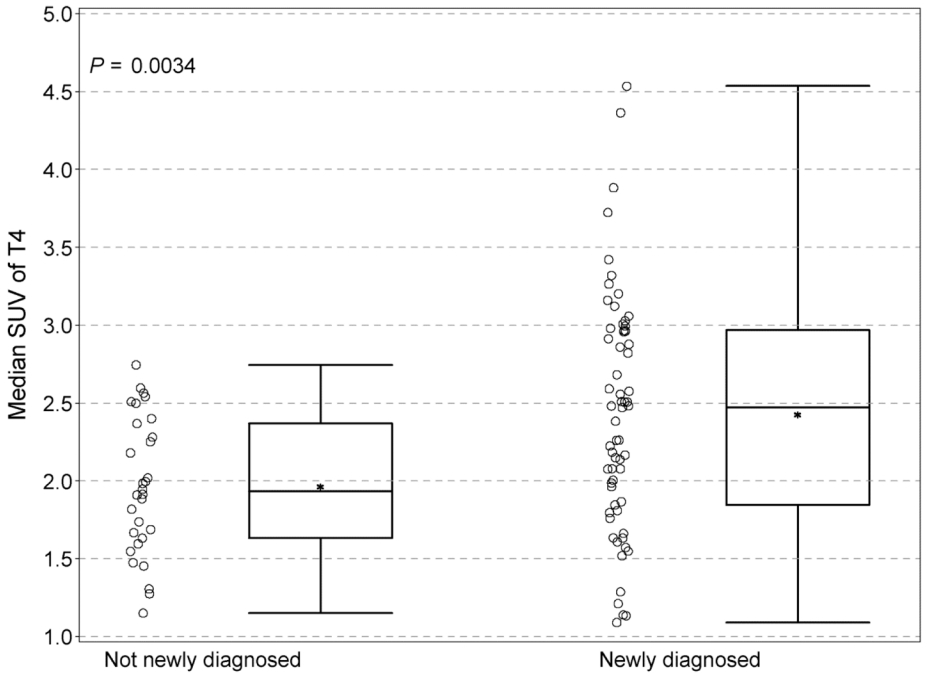

FIGURE 7.

Comparison of SUV in T4 between previously treated patients and patients at initial diagnosis before therapy. Individual data points are depicted, along with the group median (solid horizontal line in the rectangular box), the group mean (* symbol), the first and third quartiles above and below the group median (rectangular box), and the minimum and maximum SUV values (top and bottom horizontal lines).

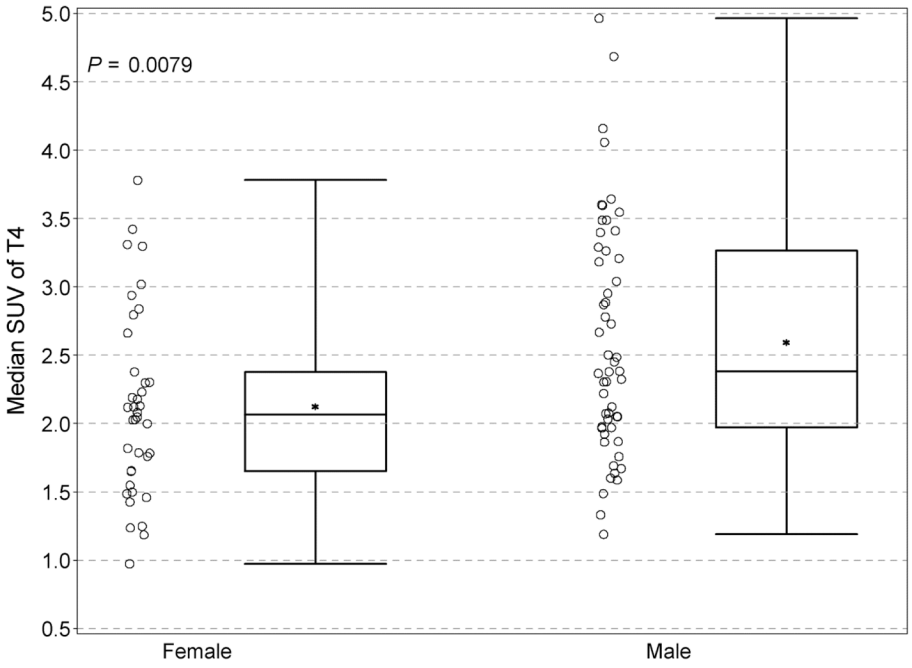

FIGURE 8.

Comparison of uptake between females and males in T5. Slightly greater uptake in both the median (*) and mean SUVmax values was present in males. Individual data points are depicted, along with the group median (solid horizontal line in the rectangular box), the group mean (* symbol), the first and third quartiles above and below the group median (rectangular box), and the minimum and maximum SUV values (top and bottom horizontal lines).

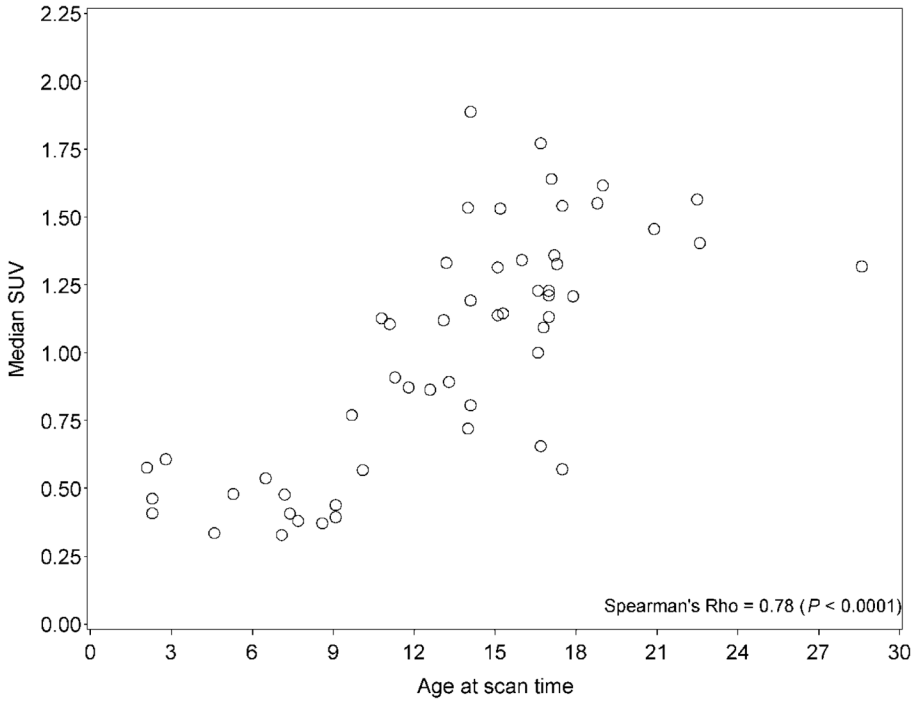

FIGURE 9.
Testicular uptake as a function of age. Individual data points are shown.

TABLE 1

Patient demographics based on sex, race, and status of diagnosis.

Characteristic	N	%
Female	38	40
Male	55	60
Whites	62	66
Others	31	34
Newly Diagnosed	62	66
Not Newly Diagnosed	31	34

N is the total patient accrual for each category. The patient total for this study was 93.

TABLE 2

A complete list of target tissues/organs encompassed by a hand-drawn region of interest.

		Median SUV				
Location	**N**	**Min**	**Q1**	**Median**	**Q3**	**Max**
Pancreas	93	4.41	9.18	12.36	14.74	22.44
Right Lobe Liver	93	4.25	7.27	8.79	10.41	20.37
Left Lobe Liver	93	4.10	6.72	8.20	9.67	15.48
Right Tonsil	92	0.74	2.70	3.60	4.48	6.83
Left Tonsil	92	1.25	2.45	3.38	4.59	7.47
Right Kidney	89	1.58	2.93	3.34	3.91	6.37
Left Kidney	91	1.79	2.78	3.20	3.81	5.96
Left Submandibular Gland	90	0.87	2.47	3.08	3.80	6.51
Right Submandibular Gland	90	1.39	2.44	2.98	3.75	5.88
Spleen	90	1.55	2.35	2.59	3.02	5.10
Right Parotid Gland	91	0.42	1.91	2.48	3.44	5.77
Left Parotid Gland	93	0.43	1.88	2.46	3.21	6.47
T6 Vertebral Body	93	1.08	2.01	2.45	2.95	5.11
Adenoids	93	0.72	1.43	2.20	3.18	5.47
T5 Vertebral Body	93	0.97	1.82	2.19	2.94	4.97
T4 Vertebral Body	93	1.09	1.76	2.18	2.68	4.54
T10 Vertebral Body	93	0.61	1.69	2.07	2.68	4.29
T12 Vertebral Body	93	0.61	1.68	2.00	2.41	4.94
T11 Vertebral Body	93	0.52	1.64	2.02	2.43	4.32
Left Vocal Cord	93	0.60	1.24	1.62	2.02	3.00
Right Vocal Cord	93	0.73	1.33	1.53	1.89	2.85
Left Ventricle Muscle	93	0.76	1.07	1.24	1.56	3.14
Right Thyroid	91	0.23	0.96	1.20	1.65	3.90
Left Thyroid	91	0.17	0.89	1.23	1.70	3.96
Right Testicle	54	0.30	0.57	1.17	1.48	2.31
Left Testicle	54	0.28	0.51	0.92	1.25	1.70
Left Ventricle Cavity	93	0.48	0.70	0.83	1.00	1.58
Left Lower Lobe Lung	92	0.37	0.60	0.78	0.92	1.24

		Median SUV				
Location	**N**	**Min**	**Q1**	**Median**	**Q3**	**Max**
Right Quadriceps	93	0.34	0.59	0.74	0.86	1.32
Right Upper Lobe Lung	92	0.44	0.61	0.70	0.83	1.42
Left Upper Lobe Lung	93	0.39	0.59	0.72	0.82	1.36
Left Quadriceps	93	0.17	0.57	0.69	0.85	1.31
Right Middle Lobe Lung	92	0.35	0.54	0.68	0.83	1.24
Right Lower Lobe Lung	93	0.34	0.53	0.64	0.78	1.04
Lingula	93	0.36	0.52	0.62	0.75	1.40

SUV = standardized uptake value; Min = minimum; Q1 = first quartile; Q3 = third quartile; Max = maximum.

J Nucl Med. Author manuscript; available in PMC 2014 November 01.

Table 3

Radiation Dosimetry

Radio Tracer	**^{11}C-Methionine**				
	Effective (mSv) & Organ Radiation Doses (mGy)				
Age (yrs)	1	5	10	15	Adult
Admin. Activity (MBq)	*145*	*225*	*407*	*720*	*740*
EDE (mSv)	*5.8*	*5.0*	*6.5*	*4.8*	*3.7*
Red Marrow (mGy)	0.6	0.5	0.6	0.7	0.6
Testes (mGy)	5.9	8.4	13.1	3.3	1.6
Bladder wall (mGy)	21.4	17.7	20.3	23.7	20.0
Kidney (mGy)	7.8	6.7	7.9	9.6	8.1
Liver (mGy)	15.0	12.1	15.5	17.2	13.3
Pancreas (mGy)	22.9	15.7	22.7	19.4	14.1
Brain (mGy)	1.0	1.2	1.7	2.5	2.5